

PAPER

High-frequency acoustic charge transport in GaAs nanowires

To cite this article: S Büyükköse *et al* 2014 *Nanotechnology* **25** 135204

View the [article online](#) for updates and enhancements.

You may also like

- [Experimental Study on the Characteristics of Acoustic Emission Source of Rock under Uniaxial Compression](#)
Zhaoyang Song
- [The deep sea Acoustic Detection system AMADEUS](#)
Christopher Lindsay Naumann and (for the ANTARES Collaboration)
- [An OpenBIM workflow to support collaboration between Acoustic Engineers and Architects](#)
Tim Pat McGinley, Thomas Vestergaard, Cheol-Ho Jeong et al.



ECS
The
Electrochemical
Society
Advancing solid state &
electrochemical science & technology

DISCOVER
how sustainability
intersects with
electrochemistry & solid
state science research

High-frequency acoustic charge transport in GaAs nanowires

S Büyükköse¹, A Hernández-Mínguez², B Vratzov³, C Somaschini²,
L Geelhaar², H Riechert², W G van der Wiel¹ and P V Santos²

¹ NanoElectronics Group, MESA⁺ Institute for Nanotechnology, University of Twente, PO Box 217, 7500 AE Enschede, The Netherlands

² Paul-Drude-Institut für Festkörperelektronik, Hausvogteiplatz 5-7, D-10117 Berlin, Germany

³ NT&D Nanotechnology and Devices, Wirichsbongardstraße 24, D-52062 Aachen, Germany

E-mail: s.buyukkose@utwente.nl

Received 19 November 2013, revised 15 January 2014

Accepted for publication 29 January 2014

Published 4 March 2014

Abstract

The oscillating piezoelectric fields accompanying surface acoustic waves are able to transport charge carriers in semiconductor heterostructures. Here, we demonstrate high-frequency (above 1 GHz) acoustic charge transport in GaAs-based nanowires deposited on a piezoelectric substrate. The short wavelength of the acoustic modulation, smaller than the length of the nanowire, allows the trapping of photo-generated electrons and holes at the spatially separated energy minima and maxima of conduction and valence bands, respectively, and their transport along the nanowire with a well defined acoustic velocity towards indium-doped recombination centers.

Keywords: acoustic charge transport, surface acoustic waves, GaAs nanowire

(Some figures may appear in colour only in the online journal)

1. Introduction

The unique properties of semiconductor nanowires (NWs) allow for the easy exploitation of quantum effects in one-dimensional systems [1], thus opening new interesting perspectives in the field of nanostructured semiconductor devices. These new possibilities are mainly based on the typically small cross-section of NWs, which favors mesoscopic size effects, and also on the removal of the constraints associated with the epitaxial growth in the case of combination of dissimilar materials. Moreover, the NW geometry allows for easy interaction with light, making them good candidates for new concepts in optoelectronic devices [2–4]. Although there are several challenges to create functional semiconductor devices for specific applications, the successful synthesis of NWs in a controllable manner, regarding both geometry and chemical composition, gives improved functionalities. For instance, radial growth for core–shell configurations [5] and axial growth for heterostructures [6] enable us to reduce unintentional surface states and to control the band structure along two directions.

In order to take advantage of their special electro-optical properties, an efficient carrier transport mechanism which eliminates the electrical contact issue on nanostructures [7] is important. In the last years, surface acoustic waves (SAWs) have proved to be a promising candidate for carrier control in two-dimensional (2D) semiconductor structures allowing both spatial and temporal manipulation: the modulated dynamic piezoelectric potential accompanying the strain field of SAWs allows spatial modulation of carriers confined in a semiconductor structure when its distance to the surface is less than the SAW penetration length. The acoustically confined carriers are then transported along the semiconductor structure with the well defined SAW velocity. This mechanism has been used for carrier as well as for spin transport over distances of several tens of micrometers in GaAs-based quantum wells [8–10].

This acoustic mechanism for carrier manipulation has recently been extended to semiconductor nanowires deposited on top of a strong piezoelectric substrate, normally LiNbO₃. The piezoelectric potential induced by the SAW can be written as $\Phi_{\text{SAW}}(x, t) = \Phi_{\text{SAW}_0} \sin[2\pi(x/\lambda_{\text{SAW}}) - (t/T_{\text{SAW}})]$, ($0 < x < l_d$). Here, Φ_{SAW_0} is the potential amplitude, T_{SAW} and

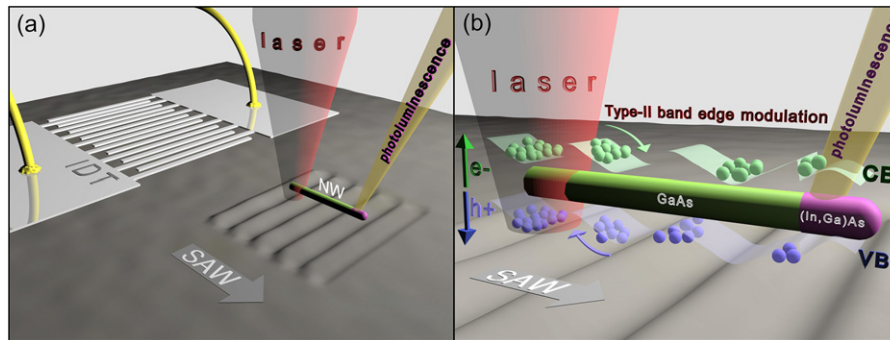


Figure 1. (a) Experimental set-up. The GaAs nanowire with a (In,Ga)As region is placed on the LiNbO₃ substrate parallel to the SAW path, with the (In,Ga)As region (violet NW section) opposite the IDT that generates the SAWs. The carriers are generated by a laser beam focused at the edge of the GaAs region (green NW section). (b) Acoustic transport mechanism: The photo-generated electrons and holes are trapped at the spatially separated and piezoelectrically induced energy minima and maxima at the conduction and valence band edges, respectively. These trapped carriers are then transported by the SAW with acoustic velocity to the (In,Ga)As region, where they recombine at quantum-dot-like centers emitting photons with energies well below those emitted by the GaAs.

λ_{SAW} are the period and wavelength of the SAW, respectively, and l_d is the carrier transport distance. In this way, acoustically induced electric currents in GaN NWs have been demonstrated [11]. Furthermore, in GaAs NWs the acoustically induced quenching of the photoluminescence (PL) [12], as well as SAW-induced ambipolar carrier transport and antibunched photon emission [13] have been reported. In all these cases, however, the carrier transport distance, l_d , was much shorter than the SAW wavelength, λ_{SAW} . Under these conditions, the piezoelectric field essentially induces a seesaw-like oscillating voltage gradient along l_d [13]. Due to this voltage gradient, carriers of opposite sign drift along opposite directions with a velocity determined by the mobility of each carrier type. The simultaneous transport of electrons and holes along the SAW propagation direction with well defined acoustic velocity, however, requires the opposite condition, that is, $\lambda_{\text{SAW}} < l_d$. For example, in the case of $l_d = 5 \mu\text{m}$ and $v_{\text{SAW}} = 3980 \text{ m s}^{-1}$ (SAW velocity for LiNbO₃), SAWs with a frequency $f_{\text{SAW}} = v_{\text{SAW}}/l_d \geq 0.8 \text{ GHz}$ must be excited to fulfill this condition.

In this paper, we demonstrate the acoustic transport of charge carriers along GaAs NWs at a frequency well above 1 GHz and over distances overcoming the acoustic wavelength (cf figure 1(a)), thus fulfilling the conditions for simultaneous transport of electrons and holes in the same direction. The SAW, generated by an interdigital transducer (IDT) fabricated on the piezoelectric substrate by nanoimprint lithography, traps the optically generated electrons and holes at different positions along the acoustic wavelength and transports them with a well defined velocity from the generation point towards the opposite end of the NW, where they are trapped by quantum-dot-like recombination centers and recombine radiatively; cf figure 1(b).

2. Experimental details

The delay line for SAW generation and transport consists of two identical IDTs fabricated on a 128° Y-cut LiNbO₃ wafer. LiNbO₃ is a strong piezoelectric material providing an intense piezoelectric field for the manipulation of carriers

in semiconductor structures placed on its surface [11–13]. In our experiments, instead of a conventional IDT design, a floating-electrode unidirectional transducer (FEUDT) design was used, which enhances the acoustic power flow in the forward direction, thus enabling higher SAW amplitudes [17]. To fabricate the IDTs, we used UV-based nanoimprint lithography (UV-NIL) combined with hydrogen silsesquioxane (HSQ) planarization and reactive ion etching (RIE) [18, 19]. In this process, first the LiNbO₃ substrate was coated with an 80 nm thick layer of WiDE-C 80 material (Brewer Science) acting as a transfer layer and 10 nm thick TranspinTM (Molecular Imprints) used as adhesion promoter for the following nanoimprint step. The substrate was then patterned by step and flash UV-NIL on an Imprio 55 tool (from Molecular Imprints) and subsequently planarized with a 160 nm thick spin-coated HSQ layer. In the following two-step RIE process, first the planarization layer was etched back in a fluorine-based plasma until the top of the imprinted features was opened. Then, using oxygen plasma, the underlying residual imprint material and transfer layer were etched down to the substrate, providing a negative side wall profile for the lift-off process. In the last step, a ~40 nm thick Al layer, sandwiched between ~4 nm thick Ti layers, was deposited and lifted off in nitric acid.

The GaAs NWs were grown by molecular beam epitaxy (MBE) using a self-assisted vapor–liquid–solid growth method [14, 15] on a Si(111) substrate. At the end of the growth process, the Ga shutter was closed and the growing surfaces were exposed to In and As fluxes for a short time. In most cases, this procedure leads to the formation of a segment approximately 300 nm in length containing (In,Ga)As at the top of the GaAs section, as indicated in figure 1. In other cases (as, for instance, for the nanowire shown in figure 2), the top region of the NW emits at the GaAs wavelength, thus indicating that (In,Ga)As is incorporated on the GaAs surface around the middle of the NW axis. Finally, an Al_xGa_{1-x}As shell with x nominally equal to 0.3 was incorporated to prevent non-radiative recombination at the free surfaces [16]. The resulting NWs had a narrow size distribution with an average length of 7 μm and diameter of 150 nm. They were then transferred from the Si substrate to the LiNbO₃ surface by

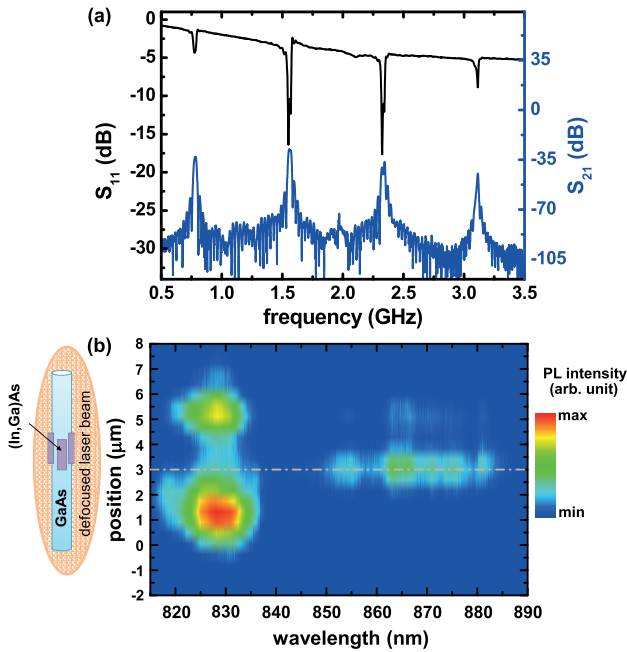


Figure 2. (a) Reflection (S_{11}) and transmission (S_{21}) coefficients as a function of the frequency of the rf signal applied to the IDT of the acoustic delay line where the NWs are deposited. (b) Photoluminescence (PL) image of NW1 under homogeneous laser illumination. The plot shows the spectroscopically resolved PL (horizontal axis) as a function of the position along the nanowire (vertical axis). $x = 0$ corresponds to the edge of the NW closest to the IDT. The (In,Ga)As recombination centers are located at $x \approx 3 \mu\text{m}$ (gray dash-dotted line). We use a logarithmic color scale.

gently pressing and rubbing the Si across the LiNbO₃ surface, along a direction parallel to the IDT delay line axis. In this way, we obtain a preferred alignment of the NWs parallel to the SAW propagation direction (cf figure 1).

The experiments on acoustic transport were performed at a nominal temperature of 20 K in a cold-finger cryostat equipped with an optical access window and coaxial connections for the application of radio-frequency (rf) signals to the IDTs. Electrons and holes are optically injected into the NW by a tightly focused (50 \times objective, spot diameter of 1.5 μm) laser beam of wavelength 756 nm placed at the edge of the NW closest to the IDT that generates the SAW. The laser pulse repetition rate was synchronized with the SAW. The NW luminescence is collected by the same objective that focuses the laser beam and sent to the input of a single grating monochromator connected to a charge-coupled device (CCD) camera for time-integrated spectroscopic measurements. The image of the SAW propagation path is parallel to the input slit of the monochromator, so that the resulting 2D image at the CCD camera shows the PL emitted by the NW with both spatial (along the NW axis) and spectroscopic resolution.

3. Results and discussion

Figure 2(a) shows the room-temperature rf power reflection (S_{11}) and transmission (S_{21}) coefficients for the IDT used in our experiments. The S_{11} spectrum shows clear minima

at frequencies fulfilling the condition $f_{\text{SAW}} = n \times v_{\text{SAW}}/\lambda_0$, n being an integer, v_{SAW} the acoustic velocity, and λ_0 the IDT fundamental wavelength. The latter is defined by the periodicity of the IDT finger grating, which in this case is 5 μm . The measurements reported below were obtained by using the second harmonic of the IDT, whose frequency at the temperature of the experiment is $f_{\text{SAW}} \approx 1.57$ GHz. This corresponds to an acoustic period of $T_{\text{SAW}} = 1/f_{\text{SAW}} \approx 0.65$ ns and an acoustic wavelength $\lambda_{\text{SAW}} = v_{\text{SAW}}/f_{\text{SAW}} \approx 2.57 \mu\text{m}$. As will be seen below, this wavelength fulfills the requirement $\lambda_{\text{SAW}} < l_d$ mentioned above for simultaneous acoustic transport of electrons and holes in the same direction with the well defined SAW velocity.

Several nanowires, grown on the same wafer and deposited on the same delay line, were studied in our experiments. Here, we show experimental results for two of them, denoted as NW1 and NW2. Figure 2(b) shows the PL emitted by NW1, in the absence of a SAW, as a function of the emission wavelength (horizontal scale) and position along the NW axis (vertical scale). The excitation was provided by a defocused laser beam covering the full NW. The PL image shows strong emission centers around 828 nm in the region $0 < x < 3 \mu\text{m}$ ($x = 0$ is defined as the lower end of the NW, the closest to the IDT generating the SAW), corresponding to the section containing the pure GaAs core. Additional, less intense, peaks at $x_r \approx 3 \mu\text{m}$ (dash-dotted line in figure 2(b)) with wavelengths above 850 nm correspond to recombination centers at the region where In is incorporated. The different emission wavelengths correspond to centers with different sizes and In concentrations. Above the In-doped region, PL emission at the typical GaAs wavelength is recovered. Similar behavior was observed for all NWs studied, with emission wavelengths for In-doped recombination centers extending to values even above 900 nm, as in the case of NW2, where the distance between the lower end and the position of the In-doped centers is $l_d \approx 5 \mu\text{m}$.

To determine the acoustic modulation efficiency at low temperatures, we recorded the PL emitted by the NWs as a function of the rf frequency applied to the IDT, when the NW is entirely illuminated by a defocused laser beam. Figures 3(a) and (b) show the detected PL emission in the GaAs segment of the NW1 for a constant rf power (P_{rf}) of 5 dBm and two different rf frequencies applied to the IDT. The rf frequency in figure 3(a) is out of the resonance of the IDT, while the one applied in figure 3(b) corresponds to the second harmonic of the FEUDT (cf figure 2(a)). The lower PL intensity in figure 3(b) is attributed to the spatial separation of photo-excited carriers in the GaAs segment of the NW due to the type II modulation of the electronic band structure created by the SAWs, as illustrated in figure 1(b). Figure 3(c) shows the spatially and spectroscopically integrated PL spectra, from the emission region marked as a dashed rectangle in figure 3(a), as a function of the rf frequency. When the frequency of the rf signal is at IDT resonance, the generated SAWs suppress about 40% of the PL emitted when the rf frequency is out of resonance.

Figure 4 shows the spatially and spectrally resolved PL emitted by two (In,Ga)As recombination centers of NW2

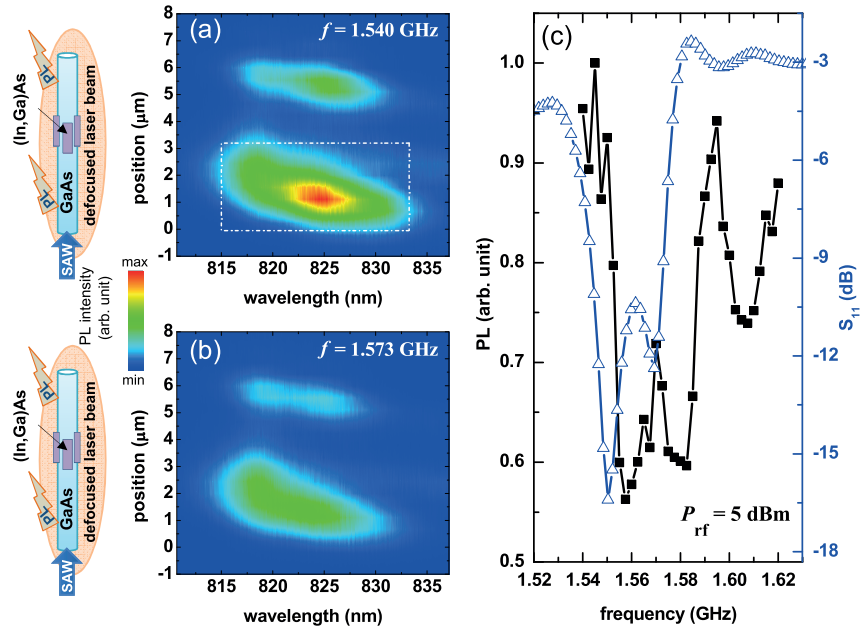


Figure 3. Spectrally (horizontal axis) and spatially (vertical axis) resolved PL images of NW1 under overall laser illumination at an rf frequency applied to the IDT of (a) 1.540 GHz and (b) 1.573 GHz. The color scale is the same in both images. (c) Rf-frequency dependence of the PL emitted by the GaAs segment of NW1 (— ■ —) (integrated in the region indicated by the dashed rectangle in (a)) and the reflection curve (S_{11}) of the IDT around the frequency of the second harmonic at room temperature (— △ —). All PL measurements were made at a nominal temperature of 20 K.

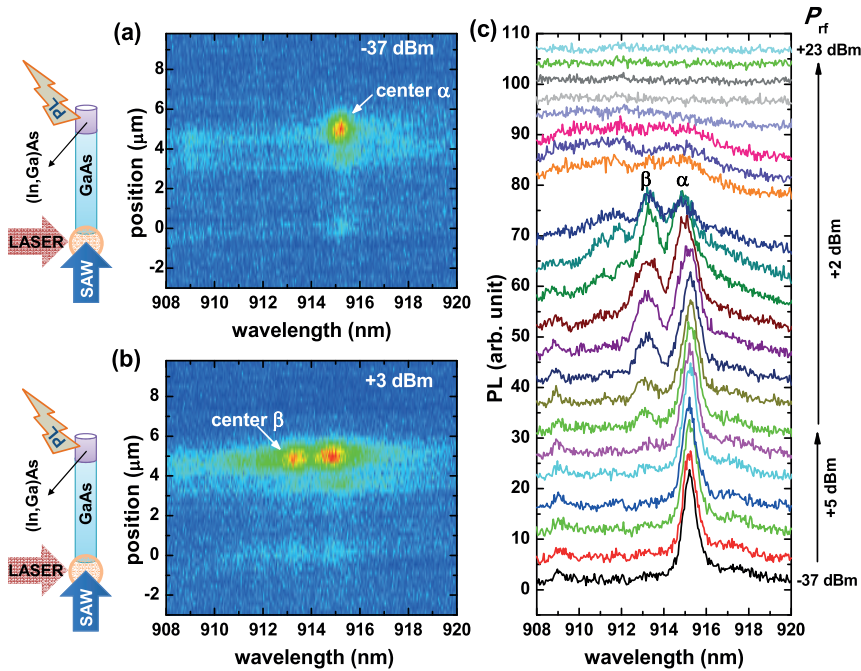


Figure 4. (a), (b) Spectral and spatially resolved images of two (In,Ga)As recombination centers at $x_r = 5 \mu\text{m}$ in NW2 under remote optical excitation by a tightly focused laser at $x = 0$, and for two powers: (a) $P_{rf} = -37$ dBm and (b) $P_{rf} = +3$ dBm. (c) Spectrally resolved PL emitted by the NW2 at x_r as a function of P_{rf} . The curves are vertically shifted for clarity.

situated at $x_r = 5 \mu\text{m}$, when carriers are optically injected by a tightly focused laser beam at $x = 0$ and acoustically transported towards x_r . For very low SAW power (cf figure 4(a)) the recombination center emitting at $\lambda_{\alpha} = 915$ nm (marked as

center α on the image) is populated by carrier diffusion along the NW. When acoustic transport is activated (cf figure 4(b)), the additional carriers transported by the acoustic wave also populate a second recombination center (marked as *center β*)

with emission energy about 2.5 meV higher than the previous one (emission wavelength $\lambda_\beta = 913.4$ nm). We probed the possible correlations between the two lines by measuring their intensity, in the absence of SAWs, as a function of the laser power used to excite the centers: we observed a non-related behavior, indicating that they are generated by independent emission centers with slightly different sizes and/or In contents.

Figure 4(c) shows the PL evolution of these two centers as a function of P_{rf} . The onset of acoustic carrier transport, determined as the rf power at which *center* β begins to emit light, is observed at $P_{rf} = -7$ dBm. Above this value, the intensity of *center* β continually increases until it reaches a maximum at $P_{rf} = 3$ dBm, and then it decreases at higher P_{rf} . PL suppression at high acoustic powers is attributed to the fact that high piezoelectric fields are able to transport carriers towards the In-doped centers, but also to detrap them, thereby preventing carrier recombination.

In order to unambiguously demonstrate that the PL modulation of figure 4 is induced by acoustic transport, we performed experiments where both the laser pulses and the rf signal are amplitude modulated (AM). By applying the same AM reference signal ($f_{AM} = 227$ Hz) to both devices, and controlling the relative phase delay between them, we can choose between the simultaneous application of laser and SAWs (*in phase*), or the introduction of a π phase delay, so that optical excitation occurs during the half period time intervals in which SAW generation is suppressed (*out of phase*). Since the heat thermalization rate in our set-up is expected to be smaller than the AM frequency, PL changes in the *out of phase* configuration are only related to the average temperature change induced on the sample by rf absorption. Measurements *in phase*, in contrast, also contain the effects induced by the acoustic transport of carriers.

Figure 5 shows the rf power dependence of the PL emitted by centers α and β for the *out of phase* (figure 5(a)) and *in phase* (figure 5(b)) configurations. In the *out of phase* case, an almost P_{rf} independent PL intensity curve is obtained. Even at high P_{rf} values, rf-induced heating is only observed as a small reduction of the PL intensity of *center* α . In the *in phase* situation, both centers show the same behavior as figure 4: a constant value for low acoustic powers, followed by a continuous increase of the PL intensity above a critical power of -7 dBm. Once the highest intensity is reached at $P_{max} = +3$ dBm, it decreases monotonically until it is totally quenched at $+19$ dBm. The intensity variation is especially pronounced in *center* β , where the acoustic transport of carriers at P_{max} enhances the PL by more than 400% with respect to the low power range.

Finally, we calculated the relative efficiency of the acoustic transport mechanism, defined as

$$r_t = \frac{I_{PL}(R)}{I_{PL}(G) + I_{PL}(R)}. \quad (1)$$

Here, $I_{PL}(G)$ and $I_{PL}(R)$ are the PL intensities collected from the generation (G) and recombination (R) regions, that is, GaAs and (In,Ga)As segments, respectively, under SAW excitation. Figure 6(a) shows the spectrally integrated PL emission from both segments of NW1 as a function of P_{rf} , while

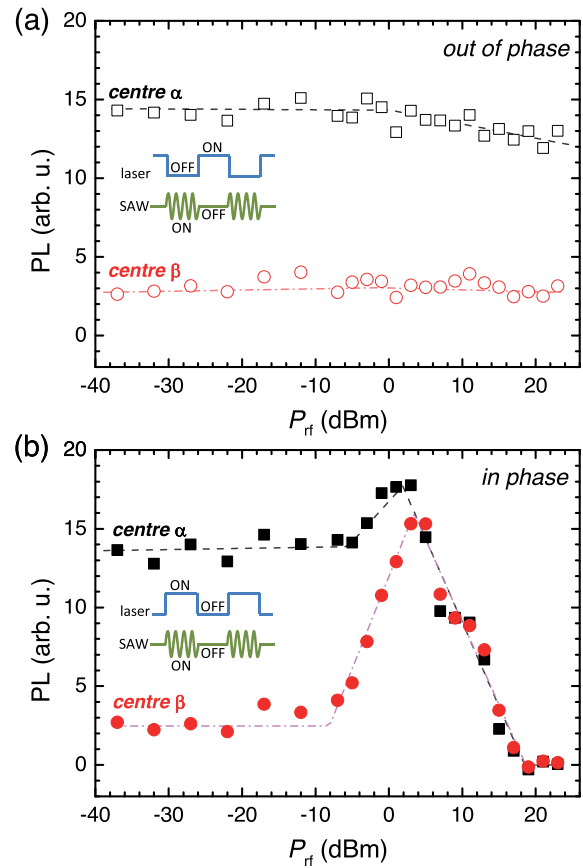


Figure 5. Spectrally integrated PL emitted by the recombination centers α and β of NW2 as a function of rf power for (a) *out of phase* synchronization of laser pulses and SAWs and (b) *in phase* synchronization. The lines are guides to the eye.

figure 6(b) shows the values of r_t estimated from figure 6(a). The small r_t for $P_{rf} < -15$ dBm is due to carrier diffusion. Between -15 and -3 dBm, the acoustically induced quenching of the PL at G due to carrier ionization, together with the enhancement of the carrier density transported towards the recombination centers at R, contribute to an increase in r_t from barely 10% to a maximum acoustic transport efficiency of about 60% in this NW. Similar results are also observed for NW2. This is very similar to the one obtained using SAWs with lower frequencies in [13, 20], indicating that the high-frequency mechanism does not diminish the efficiency of the acoustic transport process.

4. Conclusions

In conclusion, we have demonstrated carrier transport along micrometric distances in GaAs nanowires by using a high-frequency SAW ($f_{SAW} = 1.57$ GHz) that fulfills $\lambda_{SAW} < l_d$. Under these conditions, the optically generated electrons and holes are trapped at the minima and maxima of the SAW-modulated conduction and valence band, respectively, and are simultaneously transported in the same direction with the well defined acoustic wave velocity. The relative transport efficiency of this acoustic transport mechanism is about 60%,

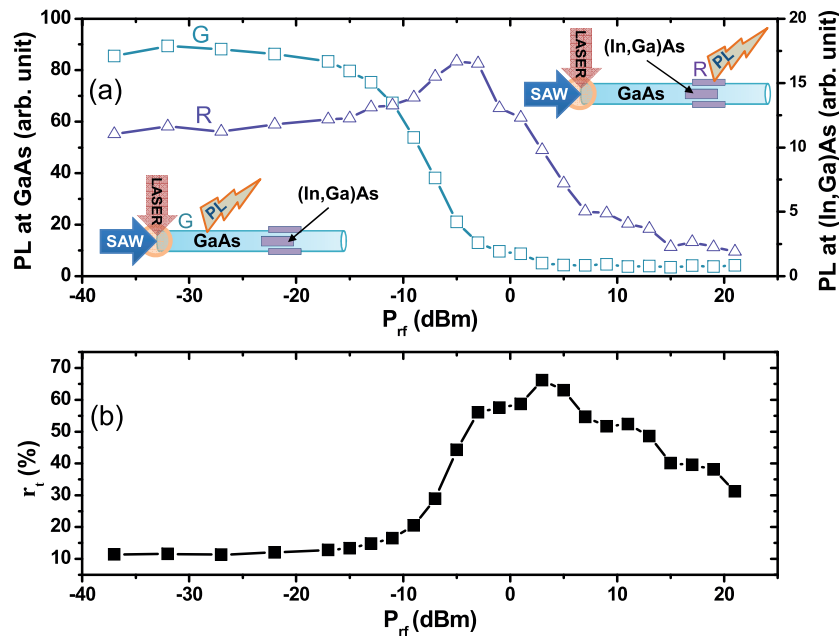


Figure 6. (a) Acoustic power dependence of the spectrally integrated PL emitted by NW1 at the GaAs carrier generation region (G) and the recombination centers in the (In,Ga)As segment (R). (b) Relative efficiency of acoustic transport, r_t , as defined at equation (1), for the centers in panel (a).

of the same order as the values obtained at lower SAW frequencies.

Acknowledgments

This research was performed within the NanoArrays project financed by The Netherlands Technology Foundation STW. We also acknowledge the financial support from the German DFG (grant GE 2224/2).

References

- [1] Yang P, Yan R and Fardy M 2010 *Nano Lett.* **10** 1529
- [2] Claudon J, Bleuse J, Malik N S, Bazin M, Jaffrennou P, Gregersen N, Sauvan C, Lalanne P and Gérard J-M 2010 *Nature Photon.* **4** 174
- [3] Holmes M, Kako S, Choi K, Podemski P, Arita M and Arakawa Y 2013 *Phys. Rev. Lett.* **111** 057401
- [4] Heiss M et al 2013 *Nature Mater.* **12** 439
- [5] Lauhon L J, Gudixsen M S, Wang D and Lieber C M 2002 *Nature* **420** 57
- [6] Gudixsen M S, Lauhon L J, Wang J, Smith D C and Lieber C M 2002 *Nature* **415** 617
- [7] Léonard F and Talin A A 2011 *Nature Nanotechnol.* **6** 773
- [8] Stotz J A H, Hey R, Santos P V and Ploog K H 2005 *Nature Mater.* **4** 585
- [9] Couto O D D Jr, Iikawa F, Rudolph J, Hey R and Santos P V 2007 *Phys. Rev. Lett.* **98** 036603
- [10] Hernández-Mínguez A, Biermann K, Lazić S, Hey R and Santos P V 2010 *Appl. Phys. Lett.* **97** 242110
- [11] Ebbecke J, Maisch S, Wixforth A, Calarco R, Meijers R, Marso M and Lüth H 2008 *Nanotechnology* **19** 275708
- [12] Kinzel J B, Rudolph D, Bichler M, Abstreiter G, Finley J J, Koblmüller G, Wixforth A and Krenner H J 2011 *Nano Lett.* **11** 1512
- [13] Hernández-Mínguez A et al 2012 *Nano Lett.* **12** 252
- [14] Colombo C, Spirkoska D, Frimmer M, Abstreiter G and Morral A F I 2008 *Phys. Rev. B* **77** 155326
- [15] Breuer S, Pfüller C, Flissikowski T, Brandt O, Grahn H T, Geelhaar L and Riechert H 2011 *Nano Lett.* **11** 1276
- [16] Ehrhardt A, Wettling W and Bett A 1991 *Appl. Phys. A* **53** 123
- [17] Yamanouchi K, Lee C H S, Yamamoto K, Meguro T and Odagawa H 1992 *IEEE Ultrason. Symp. (New York)* p 139
- [18] Büyükköse S, Vratzov B, Ataç D, van der Veen J, Santos P V and van der Wiel W G 2012 *Nanotechnology* **23** 315303
- [19] Büyükköse S, Vratzov B, van der Veen J, Santos P V and van der Wiel W G 2013 *Appl. Phys. Lett.* **102** 013112
- [20] Hernández-Mínguez A et al 2012 *MRS Proc.* **1408** BB10–42